RMetS
Royal Meteorological Society

A mixed-layer model perspective on stratocumulus steady states in a perturbed climate

S. Dal Gesso,[a]* A. P. Siebesma,[a,b] S. R. de Roode[b] and J. M. van Wessem[c]
[a]*Royal Netherlands Meteorological Institute (KNMI), AE De Bilt, The Netherlands*
[b]*Department of Geoscience and Remote Sensing, Delft University of Technology, The Netherlands*
[c]*Institute for Marine and Atmospheric Research Utrecht (IMAU), Utrecht University, The Netherlands*

*Correspondence to: S. Dal Gesso, KNMI, Wilhelminalaan 10, 3730 AE De Bilt, The Netherlands.
E-mail: gesso@knmi.nl

Equilibrium states of stratocumulus are evaluated for a range of free tropospheric conditions in a mixed-layer model framework using a number of different entrainment formulations. The equilibrium states show that a reduced lower tropospheric stability (LTS) and a drier free troposphere support a thicker cloud layer. Furthermore, cooler and drier free-tropospheric conditions promote decoupling which is the first stage of stratocumulus break-up into cumulus. The qualitative results hold for all the considered entrainment formulations, although the precise quantitative details of the boundary-layer state do vary with the choice of entrainment parametrization. Perturbations of the equilibrium states by increasing the sea-surface temperature while keeping the LTS and the free-tropospheric relative humidity constant leads to cloud thinning and an increased occurrence of decoupling regime. These results are in line with recent large-eddy simulation studies and increase the confidence in them by showing their validity for a large range of free tropospheric conditions.

Key Words: stratocumulus; mixed-layer model; entrainment parametrization; cloud–climate feedback; climate change; atmospheric boundary layer; phase-space analysis; steady states

Received 16 May 2013; Revised 12 October 2013; Accepted 17 October 2013; Published online in Wiley Online Library

1. Introduction

The importance of atmospheric boundary layer clouds for the Earth's energy balance is widely recognized. Due to their high albedo they have a strong ability to cool our planet by reflecting the incoming solar radiation. This is especially true for the marine stratocumulus (SCu) fields, that are abundant over the eastern basins of the relatively cold subtropical oceans, adjacent to the continental coasts, where the atmosphere is subjected to subsiding motions. They are characterized by a limited vertical extension of only a few hundred meters and by a strong inversion which capped them with almost discontinuous jumps of both temperature and humidity. The optical properties of SCu depend on their thickness, which is the result of a delicate balance between the surface fluxes of heat and moisture on the one hand and the cloud top entrainment that controls the fluxes across the inversion on the other hand.

Climate models exhibit a strong intermodel spread and in general tend to underestimate SCu, in terms of both cloud fraction and cloud thickness (Siebesma *et al.*, 2004; Teixeira *et al.*, 2011). This is partly the result of the coarse vertical grid spacing which is insufficient to resolve the sharp inversion. It is also related to the fact that most parameterizations of SCu in climate models do not take into account the full complexity of the interactions between many physical processes that control the cloud thickness and cloud fraction.

It therefore does not come as a surprise that the climate model representation of the cloud feedback strength of SCu is highly uncertain. Indeed, as shown by Bony and Dufresne (2005), subtropical marine boundary layer clouds, including SCu, are the main contributors to the uncertainty in the cloud radiative response to climate change among models.

In an attempt to unravel and further understand the physical mechanisms underlying these uncertainties, the CGILS* project has been set up. The framework is based on Zhang and Bretherton (2008) and is focused on three points along the GPCI† transect in the Northeast Pacific (Siebesma *et al.*, 2004; Teixeira *et al.*, 2011), each of them corresponding to a particular cloud regime: well-mixed SCu (S12), decoupled SCu (S11) and shallow cumulus, Cu (S6). For each of these locations, the cloud response to an idealized climate change has been assessed by comparing LES and SCM results for present and future climate. The considered perturbation is defined as an increase in sea surface temperature (SST) of 2 K with corresponding moist-adiabatic warming aloft and subsidence weakening, while keeping the free tropospheric

*CGILS: CFMIP-GASS Intercomparison of Large-eddy simulations (LESs) and Single-column models (SCMs);
CFMIP: Cloud Feedback Model Intercomparison Project;
GASS: Global Atmospheric System Studies.
†GPCI: GEWEX Pacific Cross-section Intercomparison;
GEWEX: Global Energy and Water cycle EXchanges Project.

relative humidity constant (Zhang and Bretherton, 2008). LES results from seven different models suggest cloud thickening for the well-mixed SCu and a slight cloud thinning for the other two locations (Blossey *et al.*, 2013). The LES results also demonstrate that the response to the perturbation has opposite effects, at least for the well-mixed SCu case: weakened subsidence promotes cloud thickening while the SST increase leads to cloud thinning. This illustrates that the net cloud feedback is a subtle one. In Zhang *et al.* (2013), SCM versions of a large number of Global Circulation Models (GCMs) have been analysed within the same framework. Contrary to LESs, the SCM results display a wide spread in cloud radiative response both in sign and amplitude. This is partly due to the choice and design of the physical parameterizations in the used SCMs but also due to the implemented numerics. In fact the SCMs have to describe the exchange of heat and moisture across the inversion, while using a relative coarse vertical resolution.

What the CGILS project did not address is to what extent the results can be generalized to a wider range of meteorological conditions and large scale forcings. The large scale forcing impact has already been addressed in Brient and Bony (2012), where stochastic variations in the subsidence are included according to the GCM statistics in order to apply more realistic large scale forcing conditions. The authors show that only in this way the sign of the cloud-climate feedback found with SCM is consistent with GCM results.

This article focusses on the dependency of the climate response to different free atmospheric conditions. The main scientific questions are the following:

1. What are the steady-state solutions of the well-mixed SCu-topped boundary layer for a wide range of atmospheric conditions?
2. How are the steady-state solutions affected by perturbations of large-scale forcings?

To this purpose we will use a mixed-layer model (MLM) framework (Lilly, 1968) which has been proven to be a powerful tool in representing realistically both the clear convective boundary layer (CBL) and the SCu-topped boundary layer (STBL) (Stevens, 2006; Zhang *et al.*, 2009). It is computationally cheaper than LES and at the same time more reliable in representing STBL than state of the art parametrizations used in GCMs (Caldwell *et al.*, 2012). Because of these advantages the MLM has already been used as a theoretical framework for various climate change studies (Caldwell and Bretherton, 2009; Caldwell *et al.*, 2012). The main limitation of MLM is that it is based on the explicit parametrization of the entrainment velocity. Various different formulations of the entrainment velocity exist and can affect the SCu cloud thickness (Stevens, 2002). In order to gain confidence in SCu response to climate change, it is important to know to what extent MLM results are affected by such a parametrization.

In section 2 the MLM theory will be summarized with a particular emphasis on various entrainment formulations. The results obtained with one specific entrainment formulation will be presented in detail in section 3, followed by the analysis of different entrainment rules. Subsequently the large scale forcings will be perturbed in order to mimic some aspects of possible future climate conditions, and the cloud response will be analysed for different entrainment formulations in section 4. Finally conclusions are collected in section 5.

2. Model framework and experiment set-up

2.1. Description of the MLM framework

As described in Stevens (2006), the MLM is based on the assumption that the layer between the surface and the inversion height, z_i, is horizontally homogeneous and vertically well-mixed. In that layer, the thermodynamic state is uniquely defined by a set of conserved variables $\psi \in \{\theta_\mathrm{l}; q_\mathrm{t}\}$ where $q_\mathrm{t} = q_\mathrm{v} + q_\mathrm{l}$ is the total water content, with q_v the water vapour content and q_l the liquid water content, and $\theta_\mathrm{l} = \theta - L_\mathrm{v} q_\mathrm{l}/c_p\pi$ the linearised form of the liquid water potential temperature, with θ the potential temperature, L_v the latent heat for condensation of water, c_p the specific heat of dry air at constant pressure and π the Exner function. These variables are governed by the turbulent fluxes at the surface and across the inversion and additional diabatic processes, ΔF_ψ, describing contributions from radiative cooling and drizzle. Large-scale forcing due to horizontal advection could be added, but is not taken into account in the present framework. The prognostic equations can then be written as (Lilly, 1968):

$$\frac{\mathrm{d}z_\mathrm{i}}{\mathrm{d}t} = w_e + \overline{w}(z_\mathrm{i}), \tag{1}$$

$$z_\mathrm{i}\frac{\mathrm{d}\psi_\mathrm{ML}}{\mathrm{d}t} = V(\psi_0 - \psi_\mathrm{ML}) + w_e \Delta_\mathrm{I}\psi - \Delta F_\psi, \tag{2}$$

where the subscripts $_0$ and $_+$ denote the surface and the height just above the inversion respectively, while the subscript $_\mathrm{ML}$ denotes the averaged value over the well-mixed layer, $\overline{w}(z_\mathrm{i})$ is the subsidence at the inversion height, $V = C_D U$ is the surface transfer velocity, where U is the horizontal wind velocity and C_D the surface exchange coefficient, w_e the entrainment velocity and $\Delta_\mathrm{I}\psi$ the thermodynamic jump at the inversion height defined as

$$\Delta_\mathrm{I}\psi = \psi_+ - \psi_\mathrm{ML}\,.$$

The steady-state solutions can be straightforwardly written as

$$\overline{w}(z_\mathrm{i}) = -w_\mathrm{e}, \tag{3}$$

$$\psi_\mathrm{ML} = \psi_0 + \frac{w_\mathrm{e}}{w_\mathrm{e} + V}(\psi_+ - \psi_0) - \frac{\Delta F_\psi}{w_\mathrm{e} + V}. \tag{4}$$

Equations (3) and (4) show that the solutions depend on the large-scale forcings, through V and $\overline{w}$, and the boundary conditions, through ψ_0 and ψ_+. To close the system, an entrainment parametrization for w_e is required. The precise physical formulation of this parametrization is crucial for determining the equilibrium solutions, as pointed out in Stevens (2002). In fact the thermodynamic state at the equilibrium is a balance between the surface and the free-tropospheric conditions and is determined by the ratio of the surface transfer velocity and the entrainment velocity. For $w_\mathrm{e}/V \ll 1$, the steady-state mixed-layer values tend asymptotically toward the surface values, while for $w_\mathrm{e}/V \gg 1$, they tend towards the free-tropospheric conditions. In conclusion, the precise value of w_e influences directly the STBL steady states.

2.2. Entrainment formulation

The entrainment velocity follows the well-known scaling relation:

$$\frac{w_\mathrm{e}}{w_*} = \frac{\eta}{Ri}\,, \tag{5}$$

where η determines the entrainment efficiency which for the CBL has been found to be constant and a good estimate is $\eta_\mathrm{CBL} = 0.2$ (Turner, 1973). Ri is the Richardson number defined as

$$Ri = \frac{z_\mathrm{i} g \Delta_\mathrm{I}\theta_\mathrm{v}}{T_0 {w_*}^2}. \tag{6}$$

Equation (6) includes the virtual potential temperature, θ_v, which is defined as

$$\theta_\mathrm{v} = \theta(1 + \epsilon_\mathrm{I} q_\mathrm{v} - q_\mathrm{l}), \tag{7}$$

with $\epsilon_\mathrm{I} = \epsilon^{-1} - 1$ and $\epsilon = R_\mathrm{d}/R_\mathrm{v}$, the ratio of the specific gas constants for dry air, R_d, and water vapour, R_v. Moreover T_0 is a reference temperature, g the gravitational acceleration and w_* a convective velocity scale which is defined as

$$w_*^3 = 2.5\frac{g}{T_0}\int_0^{z_\mathrm{i}} \overline{w'\theta'_\mathrm{v}}\,\mathrm{d}z. \tag{8}$$

In order to calculate the entrainment velocity, the buoyancy flux profile, $\overline{w'\theta'_v}$, is required.

In a STBL, in order to account for liquid water presence, the buoyancy flux is written as a linear function of the conserved variable fluxes by splitting it into the contributions of the dry sub-cloud layer and of the cloud layer:

$$\overline{w'\theta'_v} = \begin{cases} A_d\overline{w'\theta'_l} + B_d\overline{w'q'_t} & \text{if } z < z_b, \\ A_s\overline{w'\theta'_l} + B_s\overline{w'q'_t} & \text{if } z_b \le z \le z_i, \end{cases} \tag{9}$$

where z_b is the cloud-base height which is defined as the height at which the saturation specific humidity, q_s, equals $q_{t,ML}$. The so-called 'dry' coefficients, A_d and B_d, are

$$A_d = 1 + \epsilon_I q_{t,ML}\,, \qquad B_d = \epsilon_I\,,$$

and the 'saturated' coefficients, A_s and B_s, are

$$A_s = \frac{1 + q_s/\epsilon - q_{t,ML} + \gamma T_0/\epsilon}{1 + \gamma L_v/c_p}, \qquad B_s = \frac{L_v A_s}{c_p T_0} - 1,$$

where $\gamma = \mathrm{d}q_s/\mathrm{d}T$ (Stevens, 2002, gives more details).

By assuming linear flux profiles and that the radiative cooling takes place in a infinitesimal thin layer at z_i, the following expressions are found (Figure 1):

$$\overline{w'\theta'_l} = \left(1 - \frac{z}{z_i}\right)\overline{w'\theta'_{l0}} - \left(w_e\Delta_I\theta_l - \Delta F_{\theta_l}\right)\frac{z}{z_i}, \tag{10}$$

$$\overline{w'q'_t} = \left(1 - \frac{z}{z_i}\right)\overline{w'q'_{t0}} - w_e\Delta_I q_t\frac{z}{z_i}, \tag{11}$$

which shows that the scaling relation (5) is an implicit one, since $\overline{w'\theta'_v}$ depends on the entrainment velocity itself.

In order to solve this problem, the integral of the virtual potential temperature flux normalized by z_i, Θ, is introduced and the so-called process partitioning (Manins and Turner, 1978) is applied. By assuming that each physical process contributes independently to the buoyancy flux, we can split the expression into a production term that includes all the processes other than entrainment, Θ_{NE}, and a consumption term that accounts for the entrainment effect, Θ_E (Stage and Businger, 1981; van Zanten *et al.*, 1999):

$$\Theta \equiv \frac{1}{z_i}\int_0^{z_i}\overline{w'\theta'_v}\,\mathrm{d}z = \Theta_{NE} + \Theta_E\,. \tag{12}$$

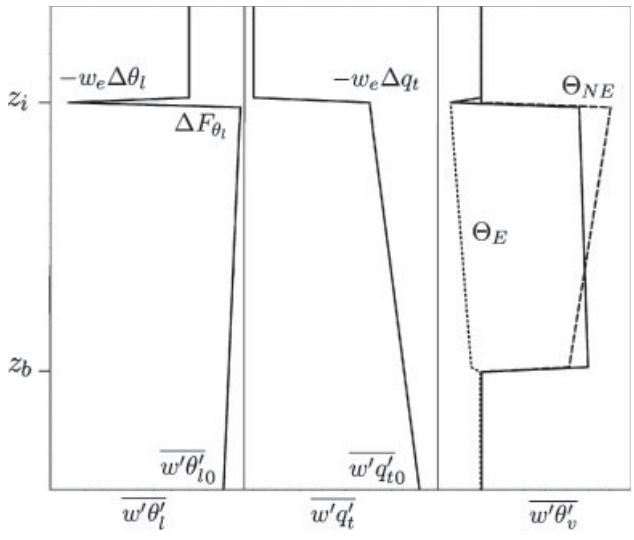

Figure 1. Sketch of $\overline{w'\theta'_l}$, $\overline{w'q'_t}$ and $\overline{w'\theta'_v}$ with process partitioning: the dotted line is the buoyancy flux due to entrainment only, Θ_E, and the dashed line is Θ_{NE} representing buoyancy flux due to all the other processes.

The contributions of Θ_{NE} and Θ_E to the integrated buoyancy flux can be written as

$$\begin{aligned}\Theta_{NE} =& \frac{1}{2}\Big\{\zeta(2-\zeta)(A_d\overline{w'\theta'_{l0}} + B_d\overline{w'q'_{t0}}) + \zeta^2 A_d\Delta F_{\theta_l} \\ &+ \left(1 - 2\zeta + \zeta^2\right)\left(A_s\overline{w'\theta'_{l0}} + B_s\overline{w'q'_{t0}}\right) \\ &+ (1-\zeta^2)A_s\Delta F_{\theta_l}\Big\},\end{aligned} \tag{13}$$

$$\Theta_E = -\frac{1}{2}w_e\Big\{\zeta^2\Delta_I\theta_{v,d} + (1-\zeta^2)\Delta_I\theta_{v,s}\Big\}, \tag{14}$$

where $\zeta = z_b/z_i$ and $\Delta_I\theta_{v,d}$ and $\Delta_I\theta_{v,s}$ are defined as

$$\Delta_I\theta_{v,d} = A_d\Delta_I\theta_l + B_d\Delta_I q_t\,,$$
$$\Delta_I\theta_{v,s} = A_s\Delta_I\theta_l + B_s\Delta_I q_t\,.$$

The process partitioning allows us, using Eq. (5), to derive an explicit expression of the entrainment velocity:

$$w_e = \frac{5\eta\,\Theta_{NE}}{2\Delta_I\theta_v + 2.5\eta\left\{\zeta^2\Delta_I\theta_{v,d} + (1-\zeta^2)\Delta_I\theta_{v,s}\right\}}. \tag{15}$$

If η_{CBL} is used for STBL, Eq. (15) underestimates the entrainment velocity as it does not account for the enhanced efficiency due to evaporative cooling. Various different strategies have been developed to include this physical process and an overview of the most common approaches is presented in the Appendix. Despite their differences, all entrainment formulations have two common features: the entrainment velocity is directly proportional to the buoyancy production term, Θ_{NE}, and is inversely proportional to $\Delta_I\theta_v$ which is a measure of the inversion stability.

In this article, we focus on the parametrization proposed by Nicholls and Turton (1986) (hereafter NT86) where the formulation (15) is used with a modified definition of $\Delta_I\theta_v$ which takes into account evaporative cooling effects (the Appendix gives details). The formulation has been tested against observational and LES data and found to give accurate results for MLM studies (Uchida *et al.*, 2010).

2.3. *Experimental set-up*

The initial conditions are taken as:
(i) the temperature near the surface is 1.5 K lower than SST;
(ii) the relative humidity (RH) near the surface is 80%.
The values of $\theta_{l,ML}$ and $q_{t,ML}$ are constant up to the boundary-layer height, which is initially set to 800 m. Where $q_{t,ML}$ exceeds the saturation specific humidity, the air is defined to be totally cloudy. Previous studies (Zhang *et al.*, 2009; Bretherton *et al.*, 2010) show that multiple equilibrium solutions are possible for the same large-scale forcings and boundary conditions. In particular, an initially clear boundary layer might remain clear. In the present work, the boundary layer is assumed to be initially cloudy as these are the solutions of our interest.

The STBL is capped with a strong thermal inversion and above the thermodynamic profiles are assumed to be steady. In order to consider a wide range of free-tropospheric conditions, the profiles are translated systematically with fixed atmospheric lapse rate for potential temperature, Γ_θ, and for humidity, Γ_q (Table 1). In particular, the specific humidity is constant in the free troposphere. By considering different free-tropospheric conditions, the jumps at the cloud top vary consequently. As an illustration, some of the considered profiles are depicted in Figure 2.

The forcings are fixed and defined according to the summer climatology of the Northeast Pacific. In particular, the SST is a typical value for SCu-topped regions and the large-scale vertical velocity, $\overline{w}(z)$, is prescribed following Bellon and Stevens (2012) as

$$\overline{w}(z) = w_0\left(1 - \mathrm{e}^{-\frac{z}{z_w}}\right), \tag{16}$$

Table 1. Large-scale forcings used in the control climate experiment (CTL) and in the two perturbed climate scenarios (PC1 and PC2).

	Units	CTL	PC1	PC2
$\Delta F_R{}^*$	$\mathrm{W\,m^{-2}}$	82.0	82.0	79.0
λ	$\mathrm{W\,m^{-2}(g\,kg^{-1})^{-1}}$	7.9	7.9	7.9
Incoming SW radiation	$\mathrm{W\,m^{-2}}$	471.5	471.5	471.5
Zenith angle	degrees	52.0	52.0	52.0
SST	K	292.0	294.0	294.0
$q_{t,0}$	$\mathrm{g\,kg^{-1}}$	13.4	15.1	15.1
p_s	hPa	1012.8	1012.8	1012.8
U	$\mathrm{m\,s^{-1}}$	6.74	6.74	6.74
w_0	$\mathrm{mm\,s^{-1}}$	3.5	3.5	3.5
z_w	m	500.0	500.0	500.0
Γ_θ	$\mathrm{K\,km^{-1}}$	6.0	6.0	6.0
Γ_{q_t}	$\mathrm{g\,kg^{-1}km^{-1}}$	0.0	0.0	0.0

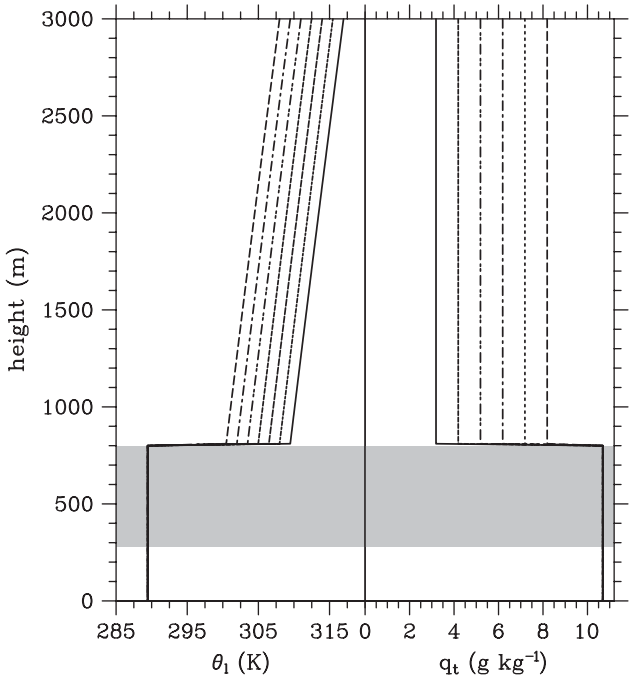

Figure 2. Some initial profiles of θ_l and q_t among the considered range of experiments. The grey area denotes the cloud layer.

where w_0 is an asymptotic value and z_w is a length-scale (Table 1 shows details). In this study, horizontal advection is neglected. Thus the set-up includes an ensemble of free-tropospheric humidity and temperature profiles for the same large-scale forcings. This permits us to isolate and investigate the contribution of free-tropospheric conditions on STBL steady states.

We will assume a non-precipitating SCu, i.e. $\Delta F_{q_t} = 0$. The effect of free-tropospheric conditions on radiative transport is taken into account by introducing $\Delta F_R = \Delta F_{\theta_l} \cdot c_p \rho$, where ρ is the air density. Based on sensitivity studies with an off-line radiative transfer code (Fouquart, 1988; Morcrette, 1991), it is approximated as a linear function of $q_{t,+}$ as:

$$\Delta F_R = \Delta F_R{}^* - \lambda q_{t,+}\,, \tag{17}$$

where $q_{t,+}$ is case dependent. Table 1 displays $\Delta F_R{}^*$ and λ which are the coefficients of the linear fit of the radiative jumps as a function of $q_{t,+}$ and estimated for the initial atmospheric state. ΔF_R is calculated for all the considered cases and then averaged for the same free-tropospheric temperature (Figure 3). In order to clarify the effect of the free-tropospheric temperature, Figure 3 comprises two grey lines which correspond to the fit for maximum and minimum free-tropospheric temperature. Therefore, as a first-order approximation, we can consider ΔF_R as a function of $q_{t,+}$ alone. Following the CGILS project (Zhang

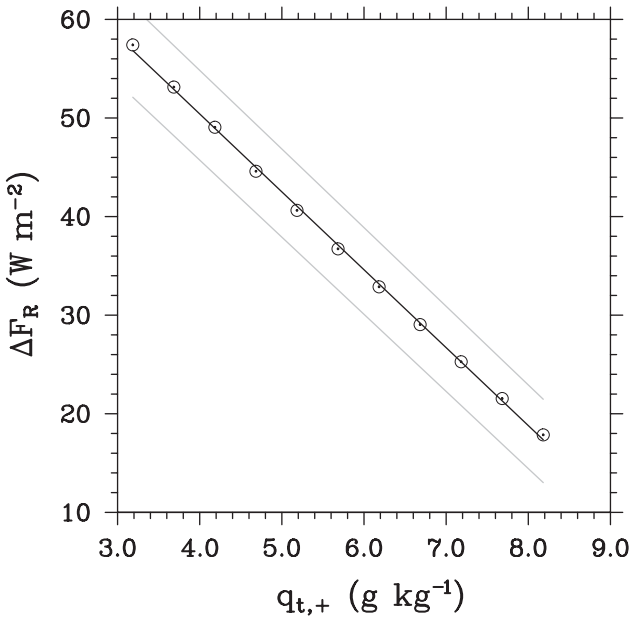

Figure 3. Considered linear fit (black line) of the radiative jump, ΔF_R, calculated with an off-line radiative code (dots) against the free tropospheric humidity values, $q_{t,+}$. The grey lines represent the fit for maximum and minimum free-tropospheric temperature.

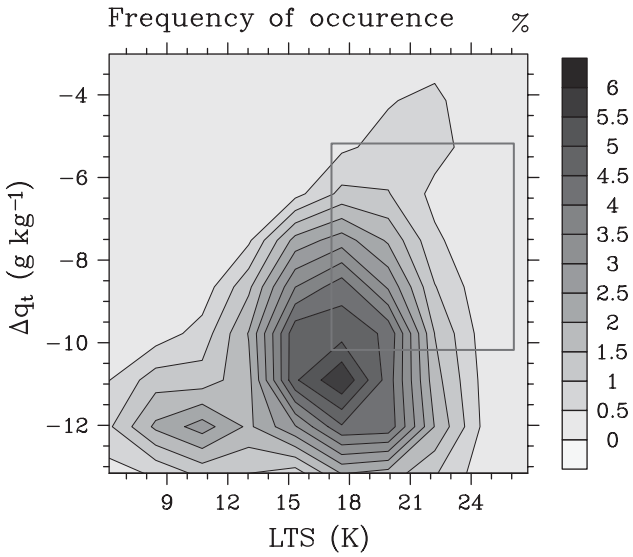

Figure 4. Probability density function distribution of night-time data from ERA-Interim for the summertime (June, July, August) between 1979 and 2012. The data are sampled in the California area of SCu (20–30°N, 120–130°W) and for the meteorological conditions corresponding to the subsidence regime and SST within 0.5 °C of the considered value. The box indicates the area of the phase space considered in the present study.

and Bretherton, 2008; Zhang *et al.*, 2013; Blossey *et al.*, 2013), the short-wave (SW) incoming radiation is set equal to the diurnally average value (more details in Table 1). The net SW contribution has been absorbed into $\Delta F_R{}^*$. We assume that changes in $\Delta F_R{}^*$ due to changes in liquid water content of the cloud layer are negligibly small. In fact, in a non-precipitating MLM, the amount of water in liquid phase is always rather large and for such high values the SW absorption saturates to a constant value.

In the upcoming sections, the STBL steady states for different free-tropospheric conditions are studied by interpreting the pattern of characteristic quantities in a phase space defined by

$$\left.\begin{aligned} LTS &= \theta(z = 3000\,\mathrm{m}) - \theta_0\,, \\ \Delta q_t &= q_t(z = 3000\,\mathrm{m}) - q_{t,0}\,, \end{aligned}\right\} \tag{18}$$

where LTS stands for lower-tropospheric stability (Klein and Hartmann, 1993) and a similar definition is used for the

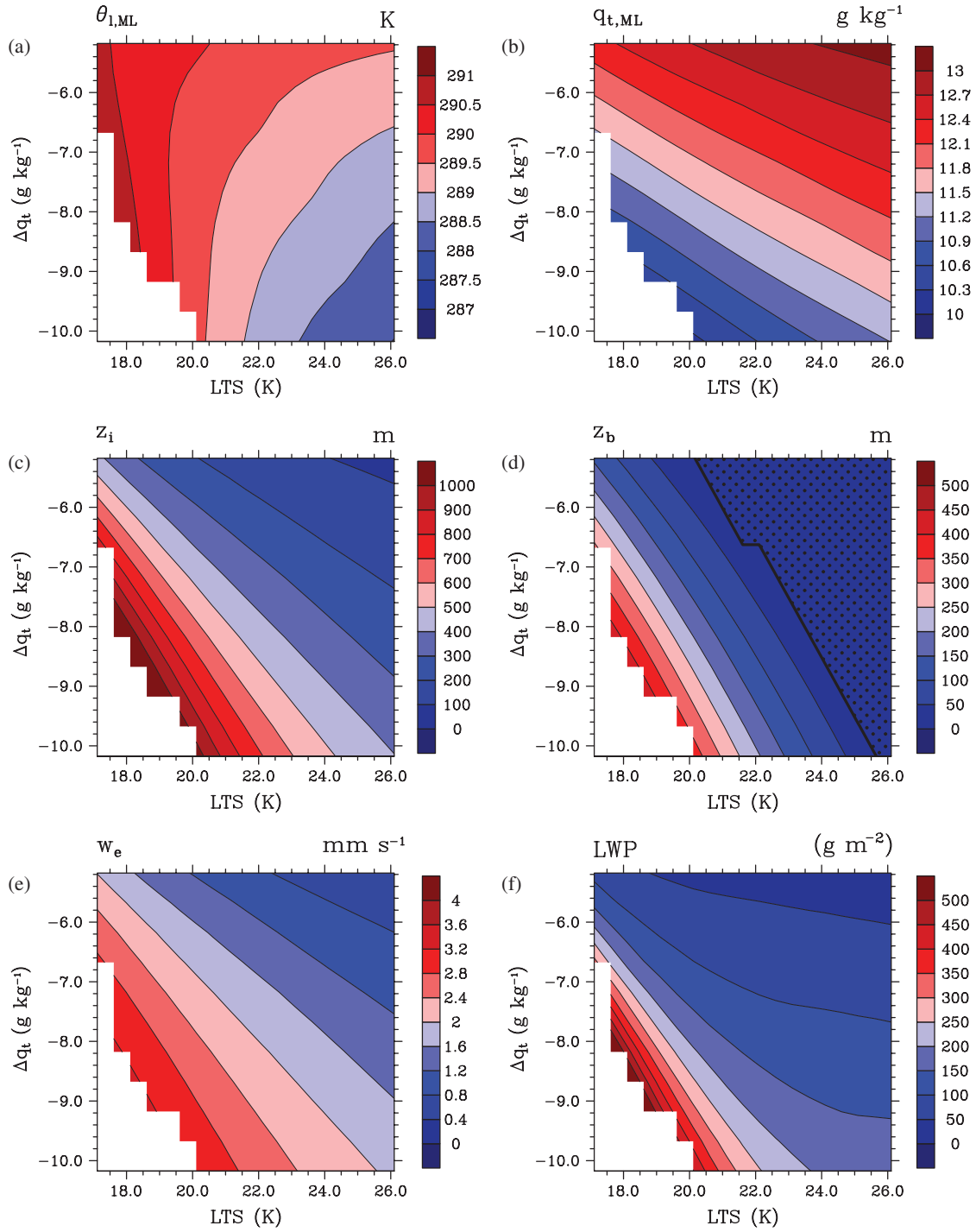

Figure 5. Phase space results from the MLM with NT86 entrainment parametrization: $\theta_{l,ML}$, $q_{t,ML}$, z_i, z_b, w_e and LWP. The white area represents the absence of steady-state solutions which is interpreted as the decoupling regime. In (d) the stippled area indicates the solutions for which the cloud base reaches the surface, interpreted as fog.

humidity, where $q_{t,0}$ is defined to be the saturation specific humidity at surface pressure and SST. An important reason to span up the phase space through the variables defined in Eq. (18) is that the equilibrium state is governed in part by the difference between surface and free-tropospheric conditions, as seen in Eq. (4).

2.4. *Suitability of the case*

In this study the following ranges are considered:

$$LTS = [17; 26]\,\mathrm{K}, \qquad \Delta q_t = [-10; -5]\,\mathrm{g\,kg^{-1}},$$

with steps of 0.5 K and 0.5 g kg^{-1}, respectively. These conditions avoid condensation in the free atmosphere and favour the presence of SCu.

To assess the frequency of occurrence of the considered ranges, LTS and Δq_t are calculated from ERA-Interim. We use night-time data for the summers (June, July and August) between 1979 and 2012, considering only the conditions with large-scale subsidence and SST within a half-degree of the value specified in Table 1. Furthermore, the data are restricted to the Californian SCu region, defined as in Klein and Hartmann (1993), i.e. 20–30°N, 120–130°W.

Figure 4 shows the joint probability density function distribution of LTS and Δq_t. The considered range, identified by the grey box, is within the possible regimes but does not include the maximum of the joint probability density function. The assumption of constant free-tropospheric total water content leads to an underestimation of Δq_t. In fact in general the observed humidity profiles show a decrease of q_t with height which would enlarge the value of the bulk jump defined in

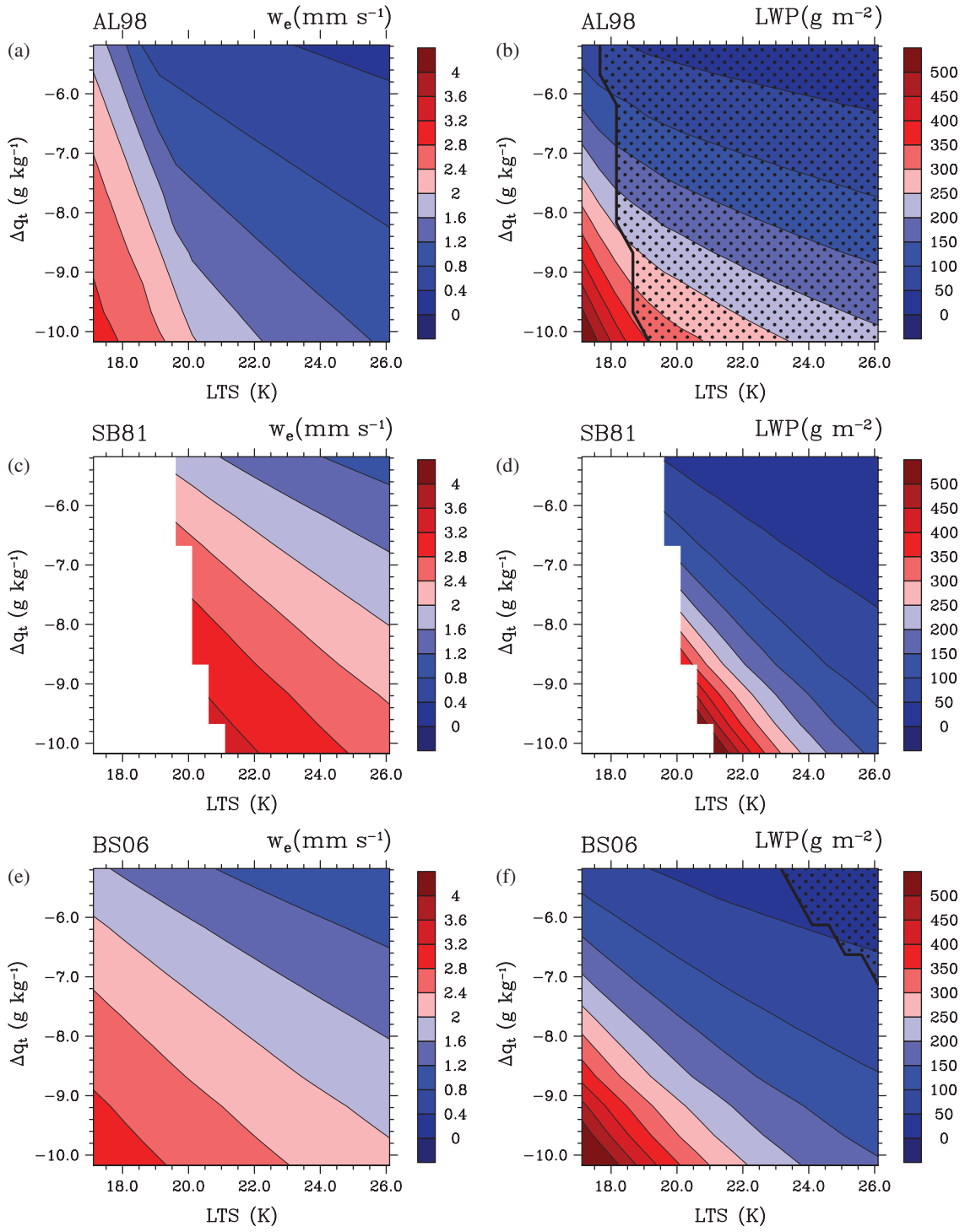

Figure 6. Phase space results from the MLM with AL98, SB81 and BS02 entrainment parametrizations; w_e and LWP are plotted for each. The white area represents the absence of steady-state solutions which is interpreted as the decoupling regime. In (b) and (f) the stippled area indicates the solutions for which the cloud base reaches the surface, interpreted as fog.

Eq. (18). Furthermore, Zhang *et al.* (2009) show that cloud fraction is lower than 20% for LTS lower than 18 K. It is then reasonable to consider only the region of the phase space where the STBL is most likely to occur.

3. SCu interaction with the free atmosphere

3.1. *Detailed analysis of steady-state solutions*

In this section, the MLM steady states using the NT86 entrainment parametrization are presented and discussed in detail. Since the steady-state solutions correspond to overcast cases with cloud fraction equal to unity, the albedo of the SCu deck depends solely on the liquid water path (LWP), which for well-mixed conditions can be written as

$$LWP = \frac{1}{2}\rho\Gamma_l(z_i - z_b)^2, \tag{19}$$

where Γ_l is the liquid water lapse rate, which is approximately constant within the cloud layer (a typical value is 2 g kg^{-1}km^{-1}). While z_i is a direct solution of the system of equations, z_b results from the thermodynamic state of the STBL and an explicit analytical expression is not derivable. Even though approximated expressions can be found in literature (e.g. Caldwell and Bretherton, 2009), in this study z_b is determined numerically as the lowest height at which $q_{t,ML}$ equals the saturation specific humidity.

If no steady states are found (i.e. z_i tendency higher than 10^{-4}m s^{-1} after 20 days of simulation), we interpret this as a sign

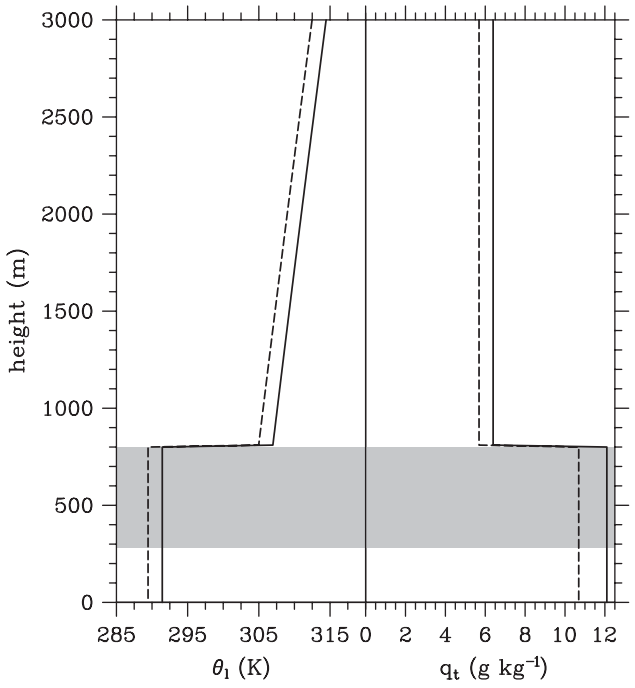

Figure 7. Initial θ_l and q_t conditions for the control climate (dashed line) and for the perturbed climate (solid line) at the centre of the phase space. The grey area denotes the cloud layer.

of decoupling for which the assumption that the STBL is well-mixed breaks down. However, the existing steady states might also be decoupled and thus not reliable as MLM solutions. Therefore an extra criterion is needed. From the assumptions that
(i) the main driving force of mixing at the cloud top is the radiative cooling;
(ii) $\Delta_I\theta_v$ is mainly determined by $\Delta_I\theta_l$,
we can diagnose the entrainment efficiency defined by Zhang *et al.* (2005), so that the entrainment velocity is

$$w_e = \frac{\eta \Delta F_R/(\rho c_p)}{\Delta_I \theta_l}. \tag{20}$$

From Eq. (9), $\overline{w'\theta_v'}$ can be approximated as $\overline{w'\theta_l'}$ in the sub-cloud layer. When η is larger than unity, the radiative cooling does not compensate the entrainment warming, so that the surface flux and the sub-cloud buoyancy flux will be both negative and the boundary layer will decouple. Hence a simple criterion for investigating the plausibility of MLM hypotheses can be defined: for $\eta > 1$ we assume that the STBL is not well-mixed and the MLM framework is not valid any more. Note that no results are shown when the STBL is decoupled, according to this definition.

The steady-state solutions of $\theta_{l,ML}$, $q_{t,ML}$, z_i, z_b, w_e and LWP are collected in Figure 5. First of all the entrainment velocity increases for weaker LTS, which is highly related to $\Delta_I\theta_l$, and is increasing for drier free-tropospheric conditions, as a consequence of the stronger radiative cooling (Figure 5(e)). Therefore the w_e pattern in the phase space can be understood on the basis of the highly simplified relation (20). Furthermore, we notice a distinct correlation with z_i (Figure 5(c)) which is a direct consequence of Eq. (3). In conclusion, the STBL deepens for weaker LTS and stronger Δq_t.

The dependency of $\theta_{l,ML}$ (Figure 5(a)) on the free-tropospheric conditions is due to the competition between entrainment warming and radiative cooling, as expressed in Eq. (4). On the left side of the phase space, where the entrainment velocity is higher, the $\theta_{l,ML}$ solutions tend towards the free-tropospheric conditions. Therefore they are mainly controlled by LTS and the STBL becomes warmer for a weaker LTS. At the same time, where the entrainment velocity is weak, a stronger dependency to Δq_t is noticeable and the STBL becomes warmer for a lower ΔF_R value (moister free atmosphere).

The pattern of $q_{t,ML}$ (Figure 5(b)) can also be understood by considering Eq. (4). On the one hand, a more stable stratification (higher LTS) prevents the dry air from above the inversion from penetrating and hence the STBL remains moister. On the other hand, the equilibrium state of $q_{t,ML}$ depends directly on the difference between surface and free-tropospheric conditions which is by construction equal to Δq_t. In conclusion, the region in the phase space corresponding to the highest $q_{t,ML}$ is located in the top-right corner, where the entrainment velocity is reduced by the stronger stratification and the air that penetrates the inversion is moister.

As already mentioned, the cloud-base height (Figure 5(d)) depends directly on the relative humidity in the mixed layer and hence depends on both $q_{t,ML}$ and $\theta_{l,ML}$. An increase in $q_{t,ML}$ promotes a lower z_b while an increase in $\theta_{l,ML}$ favours a higher z_b. Following directly from the previous discussion about $\theta_{l,ML}$ and $q_{t,ML}$, a decreasing pattern of z_b can be observed along the diagonal in Figure 5(d), with the lowest values in the upper-right corner of the phase diagram. In that region z_b reaches the surface and that can be interpreted as fog. However, note that the frequency of occurrence for the free-tropospheric conditions corresponding to the fog regime is low (Figure 4).

Equation (19) displays the dependency of LWP (Figure 5(f)) to z_i and z_b. Both z_i and z_b follow the same pattern: for a colder and drier free troposphere, the STBL becomes deeper, warmer and drier, with a consequent rise of the cloud base. However, since the LWP is proportional to the difference between z_b and z_i, the change of LWP for a colder and drier free troposphere is subtle but appears to be increasing. In conclusion, LWP increases along the diagonal from the upper-right corner to the lower-left corner.

When the cloud layer becomes deeper, drier and warmer, decoupling occurs (Wood and Bretherton, 2004), so that the well-mixed hypothesis does not hold any more. The region in which no solutions are found (white portion of the phase space) corresponds to the lower-left corner of the phase space. The entrainment velocity is enhanced for lower LTS and stronger Δq_t. These conditions promote entrainment velocity increase which destabilizes the system and leads to a negative buoyancy flux in the sub-cloud layer (Wood and Bretherton, 2004).

As decoupling is the first stage of SCu to Cu transition, we can expect a broken-cloud regime to be possible in the white area of the phase space. This is in line with the empirical relation established by Klein and Hartmann (1993). The authors found that the cloud cover is strongly correlated with LTS, and when the latter is weaker the former decreases. This consideration is important for the optical properties of the cloud deck. In fact for a SCu layer the albedo is mainly determined by LWP, while in the broken-cloud regime the cloud cover plays an important role too.

3.2. *The role of entrainment parametrization*

We will now explore to what extent the steady states depend on the specific choice of the entrainment parametrization. To this purpose, we will consider entrainment rules proposed by Lock (1998) (AL98), Stage and Businger (1981) (SB81) and the toy version introduced by Stevens (2006) (BS06); more details are given in the Appendix.

Figure 6 collects the equilibrium results of w_e and LWP for each parametrization. Interestingly the qualitative behaviour of both LWP and w_e in the phase space is independent of entrainment parametrizations and can be generally summarized as follows. For weaker LTS the entrainment velocity increases and the cloud layer thickens with a consequent LWP increase. On the other hand, the different humidity profiles in the free atmosphere lead to a variation in radiative cooling which is the main source of turbulent kinetic energy at cloud top. Thus for a drier free troposphere, corresponding to a stronger ΔF_R, the entrainment velocity is enhanced resulting in a LWP increase. It is important to stress that, even though z_i and z_b follow the same pattern, the cloud-top height variation is larger and therefore more effective

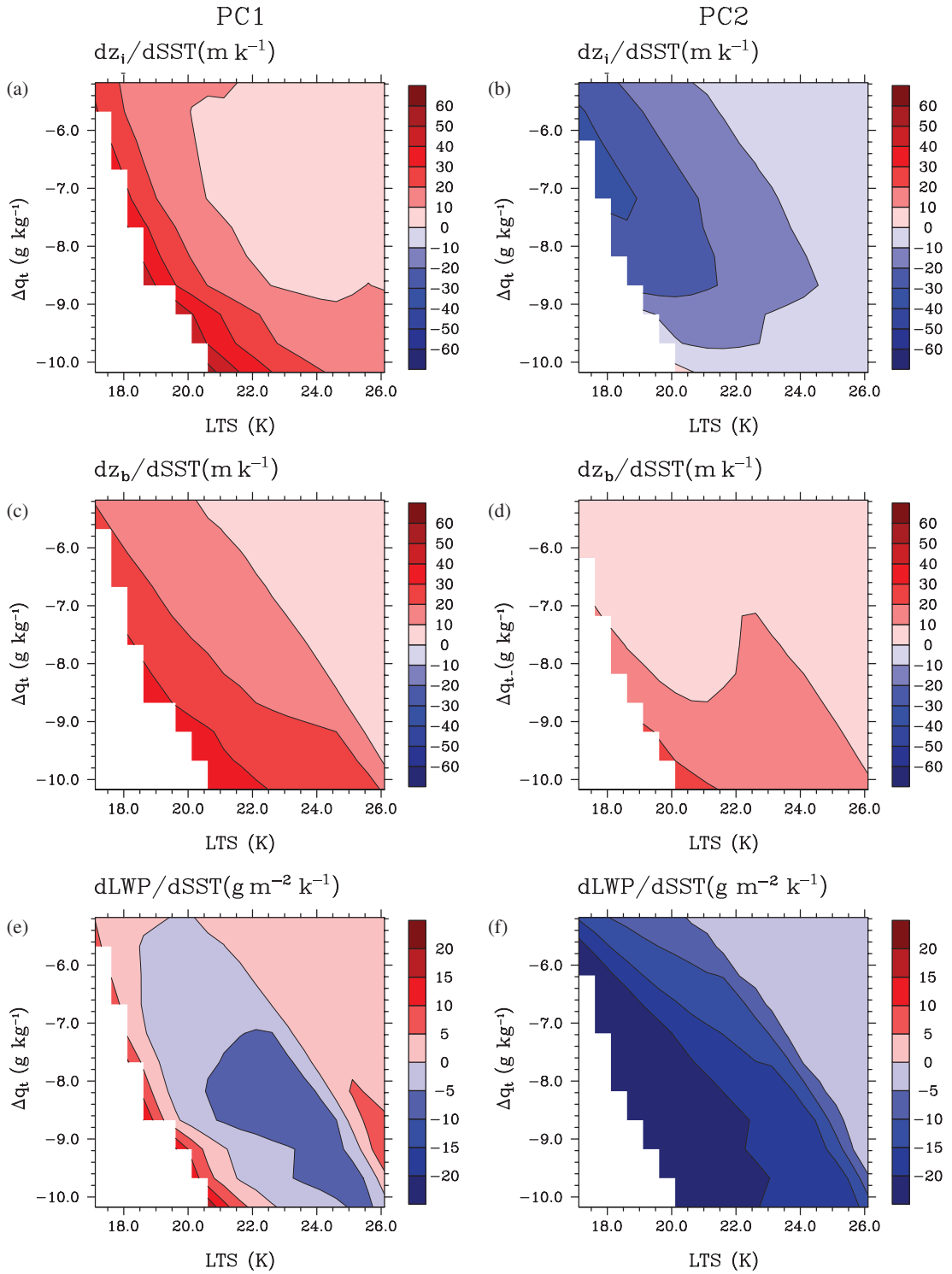

Figure 8. Phase space results from the MLM with NT86 entrainment parametrizations for both the considered climate perturbations (PC1, left column and PC2, right column): (a, b) dz_i/dSST, (c, d) dz_b/dSST and (e, f) dLWP/dSST. The white area represents the absence of steady-state solutions which is interpreted as the decoupling regime.

in determining the geometrical thickness distribution in the phase space (Caldwell and Bretherton, 2009).

At the same time, the more quantitative results do depend on the details of the entrainment formulation. The entrainment formulations that give relatively low entrainment efficiency (e.g. AL98) display a lower LWP, a relative large fraction of the phase space diagnosed as fog, and little to no decoupling. On the other hand, the entrainment formulations with a higher entrainment efficiency (e.g. SB81) give larger LWP, a cloud-base height that is always beyond the surface (no fog), and a large fraction of the phase space being diagnosed as decoupled.

Special considerations need to be made for BS06. Despite its simplicity, this formulation is able to qualitatively capture the LWP pattern in the phase space. We use a constant efficiency ($\eta_{BS} = 0.7$), therefore by definition the STBL is never decoupled. Furthermore the analytical solution of $\theta_{l,ML}$ can be written as

$$\theta_{l,ML} = \theta_{l0} - \frac{(1-\eta_{BS})\Delta F_R/(\rho c_p)}{V}.$$

The value of $\theta_{l,ML}$ is determined by the value at the surface, which is a function of surface pressure and SST only, the radiative forcing and the surface transfer velocity. In conclusion $\theta_{l,ML}$ does not depend on the free-tropospheric temperature profile but only on free-tropospheric humidity through ΔF_R. This is rather unrealistic and leads to an inaccurate description of the thermodynamic characteristics of STBL. However the

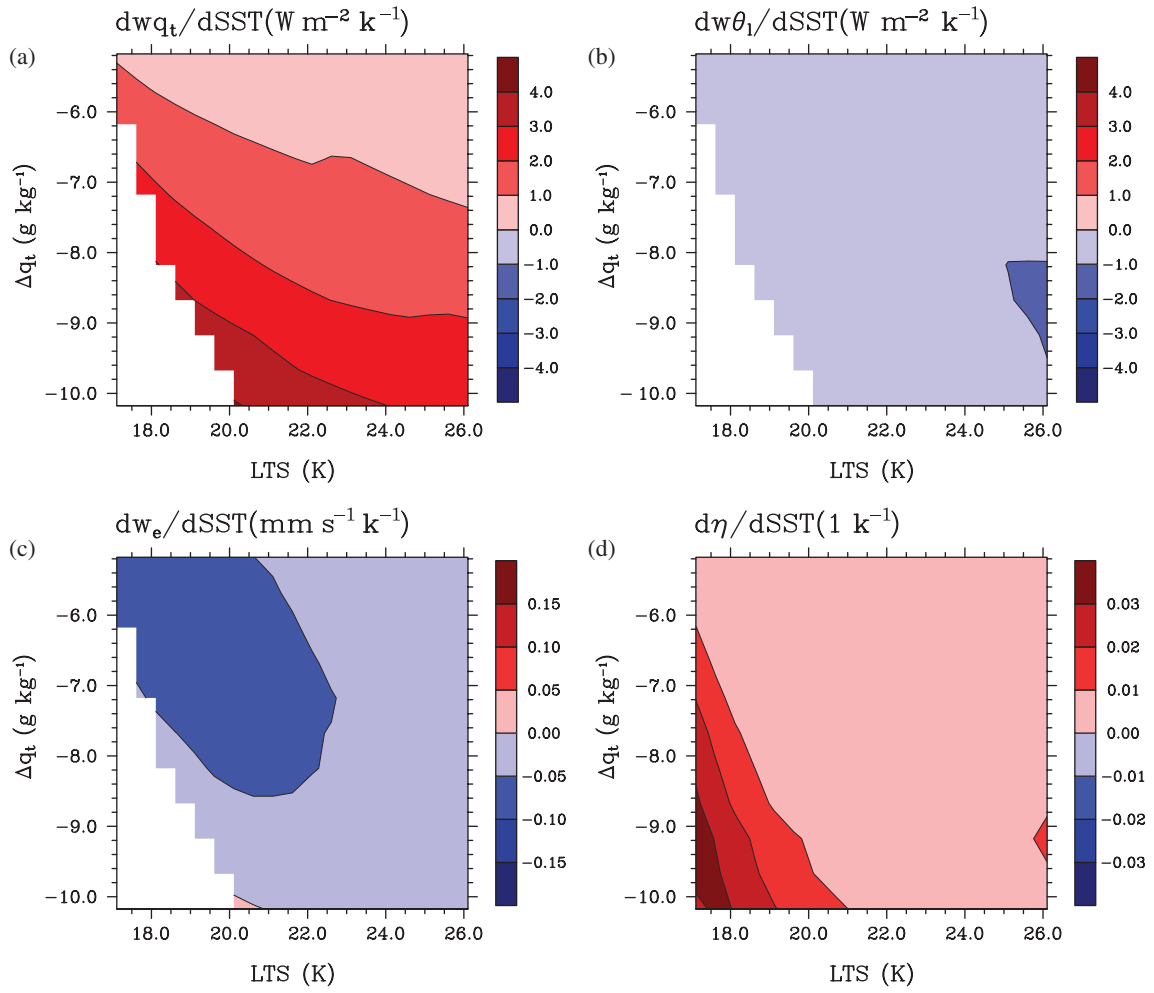

Figure 9. Phase space results from the MLM with NT86 entrainment parametrizations for the climate perturbation PC2: (a) dwq_t/dSST, (b) d$w\theta_l$/dSST, (c) dw_e/dSST and (d) dη/dSST. The white area represents the absence of steady-state solutions which is interpreted as the decoupling regime.

qualitative results are in line with the ones obtained with the more sophisticated entrainment formulations.

4. SCu response to a perturbed climate

4.1. *Climate perturbations*

In order to assess the impact of climate warming on the SCu equilibrium states, the SST is increased by 2 K. The modified STBL initial conditions are constructed in a similar way to the reference case, i.e. the initial value for $\theta_{l,ML}$ is 1.5 K lower than the increased SST and the initial $q_{t,ML}$ is chosen such as to have a near-surface value corresponding to a RH of 80%. For the free troposphere, a similar temperature perturbation is assumed. In short, the temperature profiles are uniformly increased by 2 K as in Rieck *et al.* (2012), so that the LTS remains identical to the reference case. Similarly to CGILS (Zhang and Bretherton, 2008; Blossey *et al.*, 2013; Zhang *et al.*, 2013), it is assumed that the RH in the free troposphere just above the inversion remains unaffected by the SST perturbation. Due to the imposed increased SST and the free-tropospheric temperature change, Δq_t is larger with respect to the control climate as a consequence of the Clausius–Clayperon relation. An example of the perturbed profiles is depicted in Figure 7.

Since we would like to assess the effect of change in the radiative cooling due to the humidification of the free atmosphere, two climate perturbations are considered. First we perturb the large-scale conditions as described above, keeping the radiative cooling as in the reference case (Perturbed Climate 1, PC1). To do this we compute ΔF_R using the relation (17) and the values of $q_{t,+}$ as in the control experiment. Second, we include a weakening of ΔF_R due to the increase in downwelling long-wave (LW) radiation (Perturbed Climate 2, PC2). It is worth stressing that, even though PC2 is known to be more realistic, PC1 is useful to clarify the importance of the contribution of the perturbation of radiative cooling.

In summary, the imposed perturbations encompass an increase in SST and a warming and moistening of the free atmosphere in PC1, and a consequent additional decrease in radiative cooling in PC2. A recent article by de Roode *et al.* (2014) analyses the effect of single perturbations on the STBL. The results show that a warming only of the SST leads to a growth of both cloud base and cloud top, resulting in a net increase of the LWP. A warming only of the free troposphere has the opposite effect. Furthermore increasing only $q_{t,+}$ in order to conserve RH_+ leads to a growth of the LWP. Finally a decrease in ΔF_R results in a LWP reduction. In the present set-up, all these mechanisms compete against each other in determining the sign of the LWP response. In addition, the entrainment velocity is directly affected by all of them and contributes to the final feedback. It is therefore interesting to apply simultaneous perturbations and to interpret the results on the basis of the background knowledge of single perturbations.

4.2. *SCu response to different climate perturbations*

We first discuss the results obtained by using the NT86 entrainment parametrization and in particular the variation of a variable φ due to a large-scale forcing perturbation:

$$\frac{\mathrm{d}\varphi}{\mathrm{d}SST} = \frac{\varphi|_{\mathrm{PC}} - \varphi|_{\mathrm{CTL}}}{SST|_{\mathrm{PC}} - SST|_{\mathrm{CTL}}}, \tag{21}$$

where the suffix $_{\mathrm{CTL}}$ stands for control climate and $_{\mathrm{PC}}$ for perturbed climate. It should be stressed that the variation in

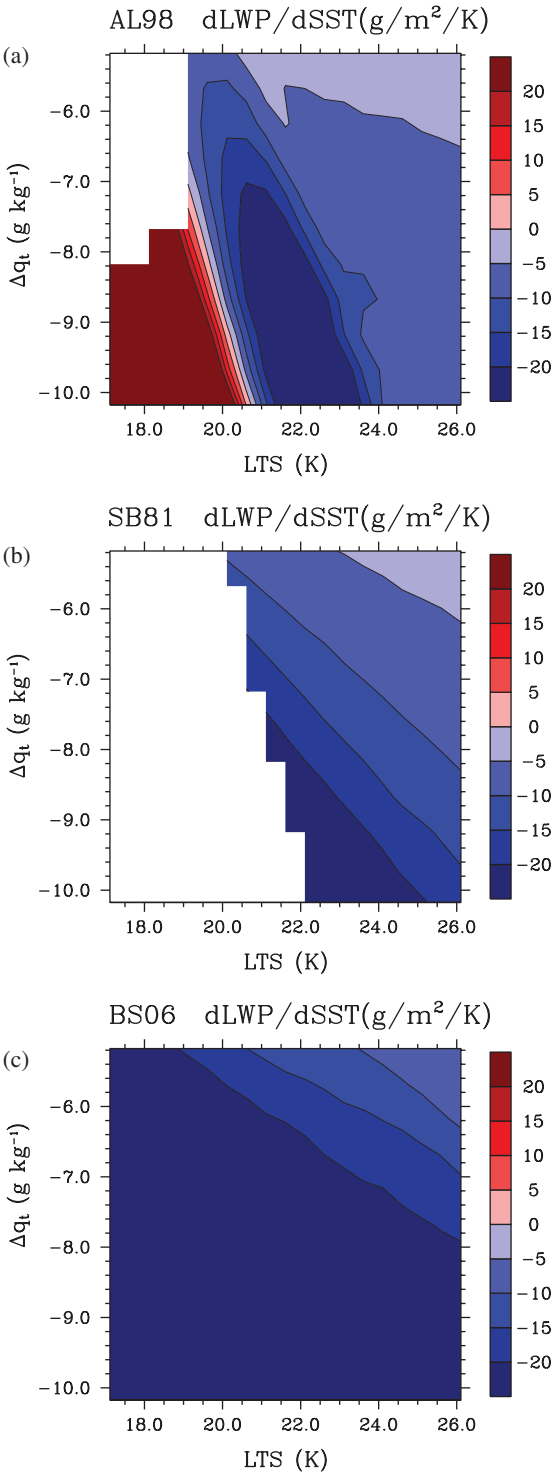

Figure 10. Phase space results from the MLM: d*LWP*/d*SST* for (a) AL98, (b) SB81 and (c) BS02 entrainment parametrizations. The white area represents the absence of steady-state solutions which is interpreted as the decoupling regime.

SST, as indicated in Eq. (21), includes also the other associated perturbations discussed in the previous subsection. To compare the effects of the different perturbations, the results are displayed in the same phase-space diagram as in section 3, labelled with Δq_t and LTS values from the *control* experiment.

In Figure 8, the responses of z_i, z_b and LWP to the two large-scale perturbations are compared. Irrespective of the radiative forcing perturbation, the STBL becomes warmer and more humid due to the direct effect of SST increase. In both cases, the moistening of the STBL is not sufficient to compensate for the warming, causing the RH to decrease and the cloud base to rise (Figure 8(c, d)). At the same time, the cloud-top height is determined by the response of the entrainment velocity. The SST increase leads to an enhancement of the latent heat flux at the surface which is an important source of turbulence within the STBL and at the inversion. While for PC1 z_i increases due to this phenomenon (Figure 8(a)), for PC2 the decrease of radiative cooling overcompensates the latent heat flux increase, leading to a z_i decrease. This result is in line with a recent observational study in which a decrease in the stratocumulus-top height for an increase in the downwelling LW radiation is found (Christensen *et al.*, 2013). As a result, the LWP response has a different sign (Figure 8(e, f)). For PC2 the results are straightforward and the final response is a cloud thinning. On the other hand, for PC1 the response is almost neutral due to a similar increase in both z_i and z_b.

Our results are in qualitative agreement with a recent LES intercomparison (Blossey *et al.*, 2013) of well-mixed SCu (S12) subjected to a similar perturbation (P2 scenario). In that study, all LES results predict a cloud thinning and (except for one LES code) a decrease in the cloud-top height. Furthermore, Bretherton *et al.* (2013) compare LES results with results obtained with a MLM which includes a full radiative scheme and a drizzle parametrization. The MLM predicts a cloud thinning as well, though it presents a slight cloud-top height increase. With our highly simplified model and perturbations, we are able to capture the same response as the majority of LESs only if the ΔF_R decrease is included. Therefore the dependency of the LW radiative cooling on the free-tropospheric humidity is an essential ingredient in SCu response to global warming. In the rest of the article, we only consider PC2 as this is the most realistic perturbation.

For PC2 we include a further analysis to better justify our previous conclusions. Figure 9 displays the response of the surface fluxes, w_e and η. In line with GCM results (Webb *et al.*, 2012) and CGILS results (Zhang *et al.*, 2013), $\overline{w'q'_t}_0$ is enhanced by the imposed climate change conditions (Figure 9(a)). On the other hand, $\overline{w'\theta'_l}_0$ decreases (Figure 9(b)), which is the direct result of a lower warming rate of the STBL than that of the SST. Interestingly these conclusions are also valid for PC1 (not shown). In fact the surface fluxes are strongly affected by the surface conditions while the radiative cooling perturbation plays a weaker role. As expected, the variation of w_e (Figure 9(c)) is consistent with z_i variation, the latter being the result of the balance between subsidence and entrainment. The change in the area where decoupling is expected is subtle. For this reason we study the variation of the entrainment efficiency, η, due to climate perturbation in Figure 9(d). In the whole phase space, η increases and we can conclude that decoupling is more likely to occur. According to Eq. (20), the definition of η, both the radiative cooling and the entrainment rate decrease but, as radiative cooling dominates, η increases and hence the area where decoupling occurs increases.

4.3. *Generalization for different entrainment parametrizations*

The previous analysis for PC2 is generalized by using the other entrainment parametrizations described in the Appendix. The LWP response (Figure 10) is qualitatively the same as NT86; the cloud-top height decreases as a consequence of the reduction of the entrainment rate, while z_b grows due to the STBL warming, which raises the condensation level. Both these changes point towards a decrease in LWP for all entrainment parametrizations considered here. At the same time, the entrainment efficiency increases in the whole phase space for all the entrainment parametrizations (not shown), leading to an enlargement of the area in the phase space where decoupling occurs (except for BS06 where it is kept constant by definition).

On the left side of the phase space, the LWP obtained with AL98 increases for an increased SST. The system switches to a different regime in which the dominant process is the increase of $\overline{w'q'_t}_0$ rather than the radiative cooling contribution. This results in an increase of w_e for weaker LTS and a consequent cloud-layer thickening. This is an example of how delicate the equilibrium between all these mechanisms is. However the common features highlighted before are strong enough to give us some confidence in this analysis.

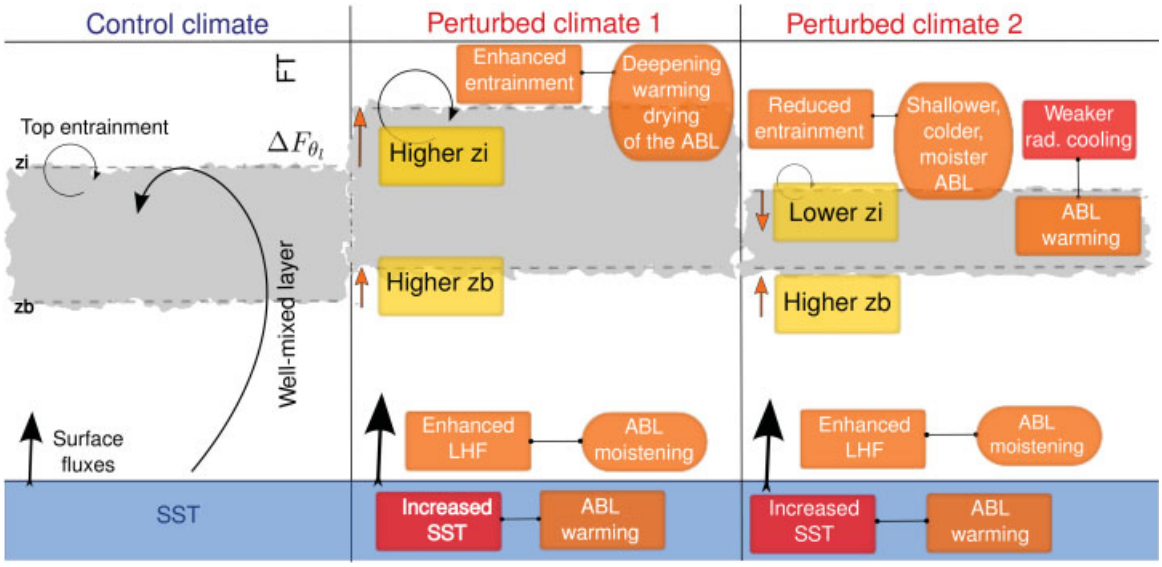

Figure 11. Schematic of the physical processes involved in a MLM (left panel), and their responses to a climate perturbation: PC1 scenario (centre panel) and PC2 scenario (right panel).

4.4. *Discussion*

To recapitulate, Figure 11 presents a schematic that summarizes the results. A sea surface warming leads to the STBL warming and moistening. The relative variation of $\theta_{l,ML}$ and $q_{t,ML}$ with respect to surface conditions affects the surface fluxes so that the latent heat flux is enhanced and the sensible heat flux is reduced. For both perturbations, the warming dominates resulting in a cloud-base rise. However the net cloud response is also affected by the change in z_i. When the reduction of radiative cooling is neglected (PC1), the entrainment is enhanced by the increased latent heat flux, the cloud top rises and the response is almost neutral. The reduction of ΔF_R has significant consequences on entrainment velocity and LWP response. If the radiative cooling is reduced, the entrainment velocity becomes smaller and the cloud top drops, leading to a cloud thinning. This result highlights the importance of radiative flux variation in a perturbed climate for STBL.

In conclusion, for the most realistic scenario (PC2), the cloud layer is predicted to thin with a consequent reduction of LWP. In terms of cloud optical properties, the decrease of LWP suggests a positive low-cloud feedback in SCu regions because less SW radiation is reflected back to space. We also need to stress that the entrainment efficiency increases, resulting in an enlargement of the region in the phase space where decoupling occurs. As decoupling is the first stage of a SCu to Cu transition, we interpret this as an increase in the occurrence of broken-cloud regime which could lead to a stronger positive feedback. Ringer *et al.* (2006) have analysed the cloud response to a uniform SST warming for different GCMs. All the models predict an increase in cloudiness for low-level clouds with high optical thickness. A similar conclusion has been drawn in Caldwell *et al.* (2012) by forcing a MLM with large-scale conditions derived from different GCMs. With our simplified model and essential set-up, we predict an opposite sign for the cloud feedback. This might have to do with the selected perturbation.

In fact the expected climate change is more complex than the one considered in this study. First of all, the increase in CO_2 is not taken into account. Including such an increase will lead to an additional increase in the downwelling LW radiation, with a consequent reduction of ΔF_R. This process will strengthen the cloud response similarly to the effect of humidity on radiative cooling. Furthermore the Hadley circulation is expected to weaken in a warmer climate with a consequent reduction in large-scale vertical velocity and a weakening of horizontal wind. The latter has a direct effect on surface fluxes and LESs and MLM results (de Roode *et al.*, 2014; Bretherton *et al.*, 2013) indicate that a reduction in wind velocity will result in a LWP decrease. In previous studies (de Roode *et al.*, 2014; Blossey *et al.*, 2013; Bretherton *et al.*, 2013), the contribution of subsidence change has been isolated and investigated. These studies suggest that weakening of the subsidence leads to a rise of cloud-top height that might be able to change the sign of the feedback leading to a SCu cloud thickening. Finally, in order to maintain the energy balance in the free atmosphere, a steepening of the moist adiabat is expected. Caldwell and Bretherton (2009) introduce the so-called subsidence–lapse rate feedback which unravels the response to this combined effect. Even though our results for control climate suggest a cloud thinning for stronger LTS, the authors find the cloud layer to thicken. As an additional sensitivity study (not shown), we have included an increase in the Γ_θ (roughly corresponding to moist adiabatic warming aloft), resulting in a LTS increase in PC2. The variation in LWP due to this extra perturbation is small compared to the effect of the radiative cooling weakening. In conclusion, the perturbations that are not included in the present work have opposite effects and the final SCu response to climate change is difficult to predict.

5. Conclusions

In order to study the SCu steady-state dependency on free-tropospheric conditions, a non-precipitating MLM coupled to different entrainment parametrizations is used. The set-up is simple and robust in order to be suitable for a range of different free-tropospheric conditions but realistic enough to be representative of the STBL. The LWP pattern in a phase space defined by LTS and a similar measure for humidity, Δq_t, is interpreted in the light of its relation with the geometrical thickness of the cloud layer. For a STBL in an equilibrium state, both z_i and z_b grow for a weaker LTS and a drier free atmosphere. This is due to the higher entrainment velocity which leads to a deepening of the STBL and a warming and drying which results in cloud-base growth. As already found in Caldwell and Bretherton (2009), the cloud top exhibits a larger variation than the cloud base, thus the cloud layer thickens following the entrainment pattern. Furthermore, when the STBL becomes deep, dry and warm, decoupling can occur. We use the entrainment efficiency η to identify the region in the phase space where this regime arises. As decoupling is the first stage in SCu to Cu transition, a broken-cloud regime can occur for a dry free troposphere and low LTS. This is in line with the experimental relation between LTS and cloud clover (Klein and Hartmann, 1993) and field campaigns such as the Atlantic SCu Transition EXperiment (ASTEX; Albrecht *et al.*, 1995).

Subsequently we have perturbed the large-scale forcings in order to mimic future climate conditions. In this work we increase the SST by 2 K while keeping both LTS and free-tropospheric RH constant. This perturbation is motivated by previous GCM studies and coincides with common hypotheses on future climate. The key role of the radiative cooling jump is assessed by considering two perturbations. A cloud thinning, consistent with recent LES studies (Blossey *et al.*, 2013; Bretherton *et al.*, 2013), is predicted only if the increase in the downwelling LW radiation due to free-tropospheric humidification is included by decreasing ΔF_R.

By analysing the results including this last perturbation (PC2), we identify a general mechanism valid for all the considered entrainment parametrizations. The reduction in radiative cooling causes the entrainment velocity to decrease and consequently the cloud top to descend. At the same time, the STBL becomes moister and warmer with respect to the control case. The cloud-base height variation is the result of the competition of these two effects and results in a cloud-base height increase. It is also worth noticing that the RH values in the sub-cloud layer decrease. In conclusion, for the more realistic scenario PC2, a positive low-cloud feedback is predicted due to both the LWP decrease and the enlargement of the region in the phase space where decoupling occurs.

We believe that this approach will be extremely useful to apply on SCM versions of climate models. The insight gained with this work is a theoretical background that can help to better understand more sophisticated models. At the same time, our conclusions should also be tested with LES models including a full radiative scheme and microphysical processes.

Acknowledgements

The research leading to these results has received funding from the European Union, Seventh Framework Programme (FP7/2007-2013) under grant agreement no. 244067. This work benefited from discussions with Roel Neggers. We also thank two anonymous reviewers for their constructive comments which have significantly improved the quality of this article.

Appendix

Nicholls and Turton (1986) (NT86) propose a parametrization which is in the same form as the general Eq. (15):

$$w_e = \frac{5\eta_{CBL}\,\Theta_{NE}}{2\Delta_I\theta_{v,NT} + 2.5\eta_{CBL}\{\zeta^2\Delta_I\theta_{v,d} + (1-\zeta^2)w_e\Delta_I\theta_{v,s}\}}.$$

The only difference is the introduction of a new definition for the virtual temperature jump, written as

$$\Delta_I\theta_{vNT} = \frac{\Delta_I\theta_v}{1 + a_2\left(1 - \frac{\Delta m}{\Delta_I\theta_v}\right)},$$

$$\text{where}\quad \Delta m = 2\int_0^1 \Delta_I\theta_v(\chi)\,\mathrm{d}\chi\,,$$

with $\Delta_I\theta_v(\chi)$ the virtual potential temperature jump caused by the mixing fraction χ, which is defined as the relative amount of free-tropospheric air mixed into a cloudy air parcel. Thus Δm is in fact proportional to the average evaporative enhancement over all the possible mixtures.

Nicholls and Turtons found $a_2 = 60$ to fit their data well, and Bretherton *et al.* (2013) claim that matches the System for Atmospheric Modelling (SAMA) LES. Nevertheless, we use $a_2 = 15$ which has been found to provide better results by McCaa and Bretherton (2004). However, the details of the NT86 entrainment parametrization do not influence the cloud–climate response (Bretherton *et al.*, 2013).

Lock (1998) (AL98) introduces an entrainment parametrization valid for $\Delta_I\theta_v > 0$:

$$w_e = \frac{2\eta_{CBL}\Theta_{NE} + \alpha_t A_s \Delta F_R/\rho c_p}{\Delta_I\theta_v}, \qquad \text{(A1)}$$

$$\text{where}\quad \alpha_t = 1 - \exp(-b_1 LWP)$$

$$\text{and}\quad b_1 = k\left(\frac{g}{T_0}\right)^{-1/3}\frac{(2z_i\Theta_{NE})^{2/3}}{(z_i - z_b)\Delta_I\theta_v},$$

where $k = 156\ \mathrm{m^2 kg^{-1}}$, an absorption factor weighted by the ratio of the cloud-top undulation height to the cloud depth.

If the saturated inversion jump satisfies the buoyancy reversal criterion, i.e. $\Delta_I\theta_{v,s} < 0$ (Randall, 1980), the formulation is written as

$$w_e = \Bigg\{ 2\eta_{CBL}\Theta_{NE}|_{\zeta=1} + 0.24\,\chi_*^2\,\Delta_I\theta_{v,s}(1-\zeta)^{3/2}\left(\frac{g}{T_0}z_i\Delta_I\theta_v\right)^{1/2} + \frac{A_s\Delta F_R}{\rho c_p}\Bigg\}\cdot(\Delta_I\theta_v)^{-1}, \qquad \text{(A2)}$$

where χ_* is the value of χ at which the parcel is just saturated.

Stage and Businger (1981) (SB81) suggest that for a CBL the ratio of Θ_E and Θ_{NE} is constant:

$$\eta_{SB} = -\frac{\Theta_E}{\Theta_{NE}}.$$

Lewellen and Lewellen (1998) and later van Zanten *et al.* (1999) find from LES results that this relation holds well for SCu and propose $\eta_{SB} = 0.35$. Using Eq. (14), the entrainment parametrization is written as

$$w_e = \frac{2\eta_{SB}\Theta_{NE}}{\{\zeta^2\Delta_I\theta_{v,d} + (1-\zeta^2)\Delta_I\theta_{v,s}\}}.$$

As the radiative cooling is actually the first source of mixing at the ABL top, while the temperature jump is the main ingredient to prevent entrainment, Stevens (2006) (BS06) introduces

$$w_e = \frac{\eta_{BS}\,\Delta F_R/\rho c_p}{\Delta_I\theta_l}, \qquad \text{(A3)}$$

where η_{BS} determines the efficiency at which free-tropospheric air is entrained in the ABL (we use $\eta_{BS} = 0.7$).

References

Albrecht BA, Bretherton CS, Johnson D, Schubert WH, Frisch AS. 1995. The Atlantic Stratocumulus Transition Experiment, ASTEX. *Bull. Am. Meteorol. Soc.* **76**: 889–904.

Bellon G, Stevens B. 2012. Using the sensitivity of large-eddy simulations to evaluate atmospheric boundary-layer models. *J. Atmos. Sci.* **69**: 1582–1601.

Blossey PN, Bretherton CS, Zhang M, Cheng A, Endo S, Heus T, Liu Y, Lock AP, de Roode SR, Xu KM. 2013. Marine low-cloud sensitivity to an idealized climate change: The CGILS LES intercomparison. *J. Adv. Model. Earth Syst.* **5**: 234–258, doi: 10.1002/jame.20025.

Bony S, Dufresne J. 2005. Marine boundary-layer clouds at the heart of tropical cloud feedback uncertainties in climate models. *Geophys. Res. Lett.* **32**: L20806, doi: 10.1029/2005GL023851.

Bretherton CS, Uchida J, Blossey PN. 2010. Slow manifolds and multiple equilibria in stratocumulus-capped boundary layers. *J. Adv. Model. Earth Syst.* **2**: 14, doi: 10.3894/jame.2010.2.14.

Bretherton CS, Blossey PN, Jones C. 2013. Mechanisms of marine low cloud sensitivity to idealized climate perturbations: a single-LES exploration extending the CGILS cases. *J. Adv. Model. Earth Syst.* **5**: 316–337, doi: 10.1002/jame.20019.

Brient F, Bony S. 2012. Interpretation of the positive low-cloud feedback predicted by a climate model under global warming. *Clim. Dyn.* **40**: 2415–2431.

Caldwell P, Bretherton C. 2009. Response of a subtropical stratocumulus-capped mixed layer to climate and aerosol changes. *J. Clim.* **22**: 20–38.

Caldwell P, Zhang Y, Klein S. 2012. CMIP3 subtropical stratocumulus cloud feedback interpreted through a mixed-layer model. *J. Clim.* **26**: 1607–1625.

Christensen MW, Carrió GG, Stephens GL, Cotton WR. 2013. Radiative impacts of free-tropospheric clouds on the properties of marine stratocumulus. *J. Atmos. Sci.* **70**: 3102–3118.

Fouquart Y. 1988. Radiative transfer in climate models. In *Physically-Based Modelling and Simulation of Climate and Climatic Change (Part I and II)*, Schlesinger ME. (ed.) *NATO ASI Series* **C 243**: 223–283. Kluwer Adademic: Dordrecht, the Netherlands.

Klein S, Hartmann D. 1993. The seasonal cycle of low stratiform clouds. *J. Clim.* **6**: 1587–1606.

Lewellen D, Lewellen W. 1998. Large-eddy boundary-layer entrainment. *J. Atmos. Sci.* **55**: 2645–2665.

Lilly D. 1968. Models of cloud-topped mixed layers under a strong inversion. *Q. J. R. Meteorol. Soc.* **94**: 292–309.

Lock AP. 1998. The parametrization of entrainment in cloudy boundary layers. *Q. J. R. Meteorol. Soc.* **124**: 2729–2753.

Manins P, Turner J. 1978. The relation between the flux ratio and energy ratio in convectively mixed layers. *Q. J. R. Meteorol. Soc.* **104**: 39–44.

McCaa J, Bretherton CS. 2004. A new parameterization for shallow cumulus convection and its application to marine subtropical cloud-topped boundary layers. Part 2: Regional simulations of marine boundary-layer clouds. *Mon. Weather Rev.* **132**: 883–896.

Morcrette J-J. 1991. Radiation and cloud radiative properties in the European Centre for Medium-range Weather Forecasts forecasting system. *J. Geophys. Res.* **96**: 9121–9132.

Nicholls S, Turton J. 1986. An observational study of the structure of stratiform cloud sheets: Part II. Entrainment. *Q. J. R. Meteorol. Soc.* **112**: 461–480.

Randall D. 1980. Conditional instability of the first kind upside-down. *J. Atmos. Sci.* **37**: 125–130.

Rieck M, Nuijens L, Stevens B. 2012. Marine boundary layer cloud feedbacks in a constant relative humidity atmosphere. *J. Atmos. Sci.* **69**: 2538–2550.

Ringer M, McAvaney B, Andronova N, Buja L, Esch M, Ingram W, Li B, Quaas J, Roeckner E, Senior C, Soden BJ, Volodin EM, Webb MJ, Williams KD. 2006. Global mean cloud feedbacks in idealized climate change experiments. *Geophys. Res. Lett.* **33**: L07718, doi: 10.1029/2005GL025370.

de Roode SR, Siebesma AP, Gesso SD, Jonker HJJ, Schalkwijk J, Sival J. 2014. The stratocumulus response to a single perturbation in cloud controlling factors. *J. Clim.* (In press).

Siebesma AP, Jakob C, Lenderink G, Neggers R, Teixeira J, Van Meijgaard E, Calvo J, Chlond A, Grenier H, Jones C, Köhler M, Kitagawa H, Marquet P, Lock AP, Müller F, Olmeda D, Severijns C. 2004. Cloud representation in general-circulation models over the Northern Pacific Ocean: A EUROCS intercomparison study. *Q. J. R. Meteorol. Soc.* **130**: 3245–3267.

Stage S, Businger J. 1981. A model for entrainment into a cloud-topped marine boundary layer. Part 1: Model description and application to a cold-air outbreak episode. *J. Atmos. Sci.* **38**: 2213–2229.

Stevens B. 2002. Entrainment in stratocumulus-topped mixed layers. *Q. J. R. Meteorol. Soc.* **128**: 2663–2690.

Stevens B. 2006. Bulk boundary-layer concepts for simplified models of tropical dynamics. *Theor. Comput. Fluid Dyn.* **20**: 279–304.

Teixeira J, Cardoso S, Bonazzola M, Cole J, DelGenio A, DeMott C, Franklin C, Hannay C, Jakob C, Jiao Y, Karlsson J, Kitagawa H, Köhler M, Kuwano-Yoshida A, LeDrian C, Li J, Lock AP, Miller MJ, Marquet P, Martins J, Mechoso CR, van Meijgaard E, Meinke I, Miranda PMA, Mironov D, Neggers R, Pan HL, Randall DA, Rasch PJ, Rockel B, Rossow WB, Ritter B, Siebesma AP, Soares PMM, Turk FJ, Vaillancourt PA, Von Engeln A, Zhao M. 2011. Tropical and subtropical cloud transitions in weather and climate prediction models: The GCSS/WGNE Pacific cross-section intercomparison (GPCI). *J. Clim.* **24**: 5223–5256.

Turner JS. 1973. *Buoyancy Effects in Fluids*. Cambridge University Press: Cambridge, UK.

Uchida J, Bretherton C, Blossey P. 2010. The sensitivity of stratocumulus-capped mixed layers to cloud droplet concentration: Do LES and mixed-layer models agree? *Atmos. Chem. Phys.* **10**: 4097–4109.

Webb M, Lambert F, Gregory J. 2012. Origins of differences in climate sensitivity, forcing and feedback in climate models. *Clim. Dyn.* **38**: 1545–1559, doi: 10.1007/s00382-011-1283-y.

Wood R, Bretherton C. 2004. Boundary-layer depth, entrainment, and decoupling in the cloud-capped subtropical and tropical marine boundary layer. *J. Clim.* **17**: 3576–3588.

van Zanten M, Duynkerke P, Cuijpers J. 1999. Entrainment parameterization in convective boundary layers. *J. Atmos. Sci.* **56**: 813–828.

Zhang M, Bretherton C. 2008. Mechanisms of low cloud–climate feedback in idealized single-column simulations with the community atmospheric model, version 3 (CAM3). *J. Clim.* **21**: 4859–4878.

Zhang Y, Stevens B, Ghil M. 2005. On the diurnal cycle and susceptibility to aerosol concentration in a stratocumulus-topped mixed layer. *Q. J. R. Meteorol. Soc.* **131**: 1567–1583.

Zhang Y, Stevens B, Medeiros B, Ghil M. 2009. Low-cloud fraction, lower-tropospheric stability, and large-scale divergence. *J. Clim.* **22**: 4827–4844.

Zhang M, Bretherton CS, Blossey PN, Austin PH, Bacmeister JT, Bony S, Brient F, Cheedela SK, Cheng A, Del Genio AD, de Roode SR, Endo S, Franklin CN, Golaz J-C, Hannay C, Heus T, Isotta FA, Dufresne J-L, Kang I-S, Kawai H, Köhler M, Larson VE, Liu Y, Lock AP, Lohman U, Khairoutdinov MF, Molod AM, Neggers RAJ, Rasch P, Sandu I, Senkbeil R, Siebesma AP, Siegenthaler-Le Drian C, Stevens B, Suarez MJ, Xu K-M, von Salzen K, Webb MJ, Wolf A, Zhao M. 2013. CGILS: Results from the first phase of an international project to understand the physical mechanisms of low-cloud feedbacks in general circulation models. *J. Adv. Model. Earth Syst.*, doi:10.1002/2013MS000246.

